Investigation on the Optimization of GaN Etching for FinFET Applications

Albert Malmros

Department of Electrical and Information Technology
Faculty of Engineering, LTH, Lund University
SE-221 00 Lund, Sweden

Supervisors: Erik Lind & Philipp Gribisch
Examiner: Lars-Erik Wernersson

June 16, 2022

LUND
UNIVERSITY

Abstract

In the framework of this thesis, the optimization of the etching process of GaN for FinFET applications has been investigated. FinFETs are transistors with a vertical architecture in the shape of fins. These fins are fabricated by etching a pattern into a GaN substrate. The etching is carried out in two steps, a dry etch and a wet etch. In this thesis, these etching steps have been carried out while different parameters have been varied. The resulting fins have been examined in a SEM. The dry etch is carried out with ICP-RIE where the RF power, ICP power, and BCl_3/Cl_2 gas ratios have been varied.

Increasing the RF power results in an increase of both physical and chemical etching components, resulting in increased etch rate and smoother fin walls. Increasing the ICP power however only increases the chemical etching component, resulting in increased etch rate but unchanged fin shape. Increasing the BCl_3 gas ratio on the other hand reduces the chemical etching component, resulting in a reduced etch rate. By pre-heating the chemical and carrying out the process in a single time interval, instead of multiple short intervals, the most complete wet etch process can be achieved. A complete wet etch results in a fin with smooth sidewalls and no rough surfaces.

The increased BCl_3 gas ratio actively worsens the etching process and the ICP power increase only affects the rate, making it a not worthwhile change to the etching process. Only the RF power increase is a worthwhile change to the etching process. A proposed optimized recipe would be ICP-RIE etching with an RF power of 120 W, an ICP power of 300 W, and a BCl_3/Cl_2 ratio of 10% BCl_3. This should be followed by wet etching in TMAH, heated to 40°C for 50 minutes.

Populärvetenskaplig Sammanfattning

Vi befinner oss i en tid av ständig digitalisering, och den teknologiska utvecklingen sker i en hög takt för att hänga med. Det här arbetet har optimerat tillverkningen av en vertikal arkitektur hos transistorer, en grundläggande komponent i elektroniska kretsar. Den här arkitekturen tar formen av långa, smala fenor i halvledarmaterialet galliumnitrid GaN. Till skillnad från vanliga horisontella transistorer, så passerar strömmen vertikalt genom dessa fenor, och genom att öka deras höjd så ökar den totala mängden ström som kan passera. Det här låter mer ström passera, per yta som transistorerna tar upp.

Det är tillverkningprocessen av just dessa fenor som är fokus i det här arbetet. Processen startar med ett basprov i galliumnitrid, och det första steget är att definera fenorna. Provet täcks med en polymer som kallas för resist. En elektronstråle efterbildar sedan ett förbestämt mönster, efter fenornas form på provets yta. Där strålen exponerar resisten så ändras dess molekylära uppsättning, molekylerna hakar fast i varandra och resisten blir svårare att lösa upp. Mönstret framkallas sedan genom att provet snabbt sänks ner i en syra som löser upp resist. Den exponerade resisten blir kvar, som en mask på provets yta.

Nästa steg är att skapa fenorna, vilket görs via etsning. Provet sätts i en kammare som förseglas o pumpas med en blandning av två gaser. Ström leds genom en spole som är virad kring kammaren. Det här genererar ett magnetiskt fält över kammaren, som i sin tur inducerar ett elektriskt fält över gasen. Med tillräckligt hög energi så kommer det här elektriska fältet att omvandla gasen till ett plasma. Ett tillstånd där molekylernas beståndsdelar skiljs åt och rör sig fritt från varandra. En spänning under provet attraherar joner, laddade beståndsdelar, från plasmat. Dessa joner reagerar med provet, vilket etsar bort material från dess yta. Masken som befinner sig på provet skyddar ytan under sig, vilket resulterar i att mönstret av fenorna etsas ut ur provet. Den här processen resulterar dock i fenor med lutande väggar och en vallgrav runt botten. Det här är negativt för deras fortsatta produktion till transistorer.

Det sista steget är att släta ut fenornas form. Provet sänks ner i en uppvärmd syra, där det lämnas under en längre tid. Syran etsar bort ojämnheter lägs fenornas väggar, vilket resulterar i raka fenor med släta väggar. Det här steget förstorar dock också vallgraven runt fenorna.

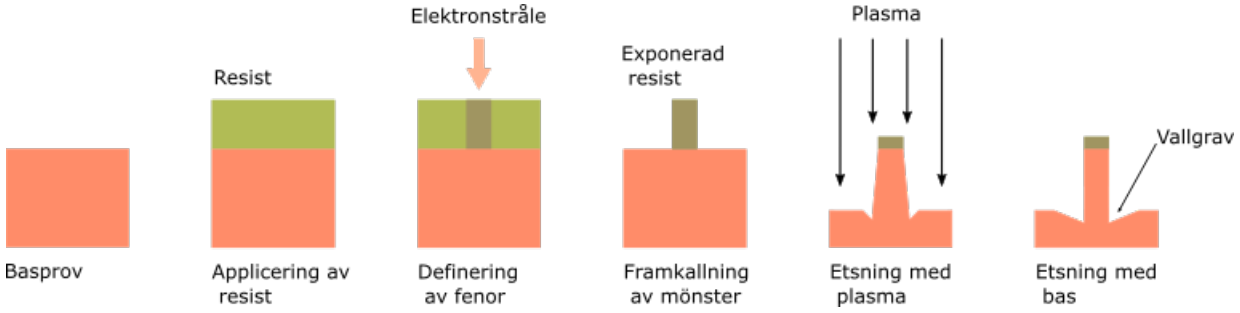

Diagram över stegen under fenornas tillverkningsprocess.

Under arbetet så har variationer av den här processen utförts på flertalet prov. Effekterna hos strömmen som omvandlar gasen till ett plasma och spänningen som attraherar plasmat till provet har varierats, förhållandet mellan de två gaserna har varierats, och tiden provet etsat i uppvärmd syra har varierats. Ett slutgiltit recept för processen har föreslagits för att skapa de bästa möjliga fenorna.

Acknowledgements

To start with, I would like to thank my supervisor, Prof. Erik Lind of the Department of Electrical and Information Technology at Lund University, for providing me his support, guidance, and knowledge. I would also like to give a special thanks to my practical coach, Philipp Gribisch, for all the hours he spent in teaching me the many different steps of the process, and for helping me along the creation of this thesis. I could never have completed this thesis without the help of you two, and I am sincerely grateful to have had this opportunity to work with you on it.

I would like to extend a thanks to Prof. Vanya Darakchieva and to Rosalia Delgado Carrascon at Linköping University, for providing the base samples that I have used for this thesis.

I would like to acknowledge Myfab for support and for access to the nanofabrication laboratory at Lund University. I would also like to thank the team at Lund Nano Lab for all the help you have provided at this laboratory.

Finally, I must give my thanks and gratitude to my friends and colleagues. To Erik and Yang whom I shared an office with, your company made the process of working on this thesis truly enjoyable. To all my friends, who throughout my many years here at Lund have provided me with endless support and inspiration. I truly appreciate it.

Thank you!

Albert Malmros

Contents

1 Introduction

Today we find ourselves in a world of ever-increasing digitalization. Computers are growing more complex and more electricity than ever is needed and consumed for daily life. With this ever-growing need for more complex electrical systems and devices, the technology that underpins it must further modernize to keep up.

The vertical fin field-effect transistor (FinFET) is a transistor created with a vertical architecture, allowing higher packing density and therefore further scaling compared to regular MOSFETs [1]. This fin shaped architecture also has advantages for the properties of the actual transistor as well. The large surface of the fin architecture allows for greater heat dispersion, and the fin shaped channels, surrounded with allow for a superior gate control [1]. Furthermore, the architecture allows for selective-area doping. Allowing for a greater performance and reliability for the transistor, as well as allowing for the the formation of selective-area p-n junctions [1].

FinFET devices are among the most successful device concepts in recent time, with applications ranging from deeply scaled technology nodes [2] to power semiconductor devices [3]. The transistor properties of particular interest in power semiconductor devices is a low on-resistance, low switching loss, and high breakdown voltage [1]. A material that has arisen as one of interest for the fabrication of semiconductor power devices is the III/V wide-bandgap (WBG) semiconductor material gallium nitride. Compared to its Si counterpart, GaN has three main advantages for these applications: Its wide bandgap, its wide breakdown field, and the high mobility of GaN channels [4]. The wide bandgap of GaN allows for a larger power density through the device, allowing GaN devices a stable operation at much higher temperatures than a Si counterpart [4]. A larger breakdown field means that a device of GaN can withstand a higher voltage, without transistor action breaking down. The higher mobility means that the semiconductor resistivity of the device is lowered.

The architecture of the FinFET device is as the name suggests, vertical, in the shape of a fin. The core of the fin is composed of n-GaN, acting as the channel through which the controlled current of the transistor can flow. The n-GaN core of the fin has a gate placed along its sides and a source contact placed on top [5]. The fin structures are very thin, on the scale of a few hundred nanometers. At a scale this small, all the electrons in the fin can be depleted by the difference in work function between the n-doped fin and the gate surrounding it [5]. With the channel depleted, it cannot carry a current, meaning that such a device will have a normally-off operation.

Creating vertical structures means that the transistor device can utilize an extra spatial dimension. A higher packing density is in this way achieved. This higher density allows for more powerful devices to be fabricated as more transistors can now fit in the same area. The vertical architecture also allows for the breakdown voltage of the device to be increased without also increasing the area of the transistor. For most transistors, the breakdown voltage can be increased by increasing its drift layer thickness, but the method for doing so differs depending on the architecture. In a vertical structure, the drift layer can be increased upwards. Essentially making it independent from the size of the device [4].

In this thesis, the fabrication process of the fins that make up this vertical architecture will be explored. Starting with a GaN sample substrate, the fins are fabricated by following a few steps. First, the sample is covered in a resist, which is patterned into the shape of the fins with electron beam lithography. Then the samples are developed, followed by dry etching with inductively coupled plasma-reactive ion etching. Following the dry etch, the samples are wet etched by submerging them in a heated base for a time.

The purpose of this thesis will be to optimize the etching process of the GaN fins, allowing the benefits of the vertical architecture to be utilized to a higher degree. This will be done by etching the fins under varying conditions. For the dry etch, the RF power, ICP power, and BCl_3/Cl_2 gas concentration will be varied from an original recipe. This will influence the shape of the fins. For the wet etch, the etching time

will be varied from an original recipe. The resulting fins will then be measured and analyzed with electron beam lithography, allowing for an optimal recipe to be suggested.

Finally, a simulation of the electric field through the architecture will be carried out in COMSOL to aid in the analysis of the results.

2 Theory

This section will cover the theoretical background of the thesis. The methods used for the fabrication and analysis will be presented and the physics, as well as the chemistry behind them, will be explained.

2.1 Sample Fabrication

This section will explore the methods that are used during the sample fabrication process. It is these methods that will be optimized in this thesis.

2.1.1 Electron Beam Lithography

Most of this section is based on the chapter on electron beam lithography by Nezih Pala and Mustafa Karabiyik, from the book "Encyclopedia of Nanotechnology" [6].

Electron beam lithography (EBL) is a precise method for patterning a sample, allowing a detailed structure to be etched out of it. The EBL process can be divided into three distinct steps. First, a thin film of resist is applied over the sample. Then this resist is exposed with a controlled electron beam, scanning along a certain pre-programmed pattern. Finally, the exposed sample is developed, removing exposed or unexposed resist (depending on type of resist) to reveal the pattern. This pattern is used as a mask, allowing the sample to be etched according to the pattern.

The exposure step of the EBL process is what sets it apart from optical processes. Instead of focusing light into a beam a device known as an electron gun generates a beam of electrons. This beam is then passed through a column, focusing and aligning the beam allowing it to be used for patterning. Using electrons for patterning allows the process a very high theoretical resolution limit. The kinetic energy of an electron can be calculated with equation 1.

$$E_{Kin} = \frac{1}{2}mv^2 \tag{1}$$

This gives a direct relationship between the wavelength of an electron to its kinetic energy, via de Broglie's famous equation, equation 2:

$$\lambda = \frac{h}{mv} \tag{2}$$

This relationship takes the form:

$$\lambda = \frac{1.23}{\sqrt{E_{Kin}}}[nm] \tag{3}$$

In equation 3 a relationship between the kinetic energy of an electron and its wavelength is established. Essentially a relationship between the energy of the electrons in the beam of the EBL system and the theoretical maximum patterning resolution. The actual resolution, while small, is also further limited by the actual EBL system. Different iterations of this system can be quite varied and complex, but functionally

they are all variations of a typical EBL system. A schematic of this typical EBL system can be seen in figure 7.

The first part of the EBL system is the source of the beam, the electron gun. The one used in this thesis is a so-called field emission gun. This consists of an extremely sharp tip, fabricated in a material with a low work function together with an anode. This anode exerts a high electric field over the gun, which concentrates in the sharp tip. The low work function of the material then allows for electrons concentrated in the tip to be extracted into a beam [6]. As the gun acts as the source for the beam used in the EBL system it is expedient that it generates a beam that is as consistent and bright as possible. Intensity, stability, uniformity, spot size, and lifetime are therefore all qualities of extra importance for the gun.

Through the EBL system, this beam will pass through a system of lenses. However, regular lenses do not work on an electron beam. Instead, electromagnetic lenses are used. These lenses utilize Coulomb's and Lorentz's law, described in equations 4 and 5, respectively [7][8].

$$\mathbf{F}_C = -q\mathbf{E} \tag{4}$$

$$\mathbf{F}_L = -q(\mathbf{E} + \mathbf{v} \times \mathbf{B}) \tag{5}$$

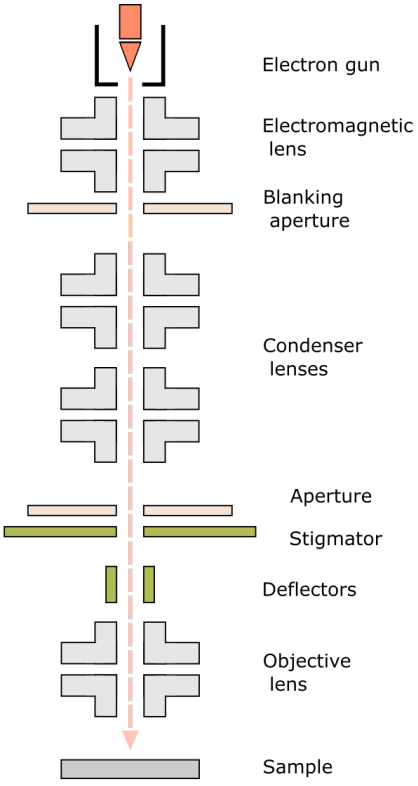

Figure 1: Schematic of a typical EBL system [6].

Equation 4 describes the force $\mathbf{F}_C$ over an electron when an electric field $\mathbf{E}$ is applied over it, along the direction of the field. q is the electron charge. Equation 5 describes the force $\mathbf{F}_L$ over an electron as it passes through a magnetic field $\mathbf{B}$ with velocity $\mathbf{v}$ when the electric field $\mathbf{E}$ is applied over it. Perpendicular to the direction of the magnetic field as well as the velocity.

These two laws describe how a force can be applied over electrons, allowing the trajectory of the beam to be controlled. Usually, both effects are not utilized at the same time, instead, two different kinds of electromagnetic lenses are used. Electrostatic lenses utilize a system of three plates along the direction of the beam, as seen in figure 2(a). The middle plate having a variable potential and the other two being grounded. As the electron beam passes through the field generated between these plates, its trajectory is altered. Thanks to the force exerted on the electrons, as described by Coulomb's law. The distribution of the electric field is inhomogeneous around the plates. It is weaker further away from the plates. Therefore a beam of parallel electron trajectories passing through an aperture of these plates will focus in a single spot after the lens. A magnetic lens instead consists of a magnet coiled around the beam axis. As the electron beam passes through it a force is exerted on the electrons, as described by Lorentz's law. The distribution of the magnetic field in the lens is inhomogeneous. It is weaker further away from the magnets, eg. in the center of the lens. Resulting in the beam of parallel electron trajectories focusing in a single spot after passing through the lens.

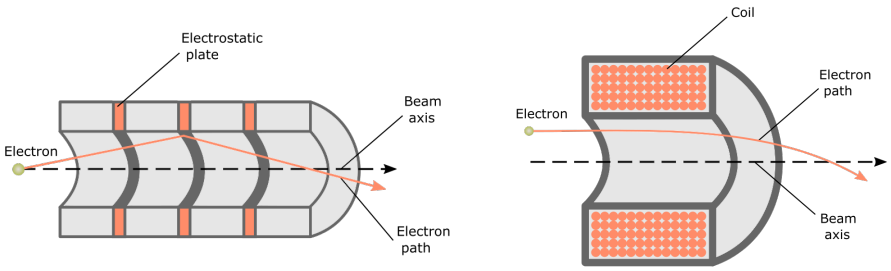

(a) Electrostatic lens (b) Magnetic lens

Figure 2: Schematic of the electromagnetic lenses used in a typical EBL system. Figure (a) shows a electrostatic lens. Figure (b) shows a magnetic lens [6].

Besides the lenses, there are a few more parts to the typical EBL system. Apertures, stigmators, and deflectors. The apertures set the convergence angle of the beam passing through it, by limiting some of it. Some apertures also totally stop the beam by applying a voltage to a plate, deflecting the beam away from the aperture opening. This is done because shutting off the beam and turning it on again would comparatively be wildly inefficient. The stigmator is used to counteract a common issue in systems based on lens operations, astigmatism. A phenomena that distorts the shape of the beam cross-section.

This patterning is done on a layer of photoresist covering the surface of the sample. This resist is a chemical consisting of long, often carbon-based, polymer chains. The reason these materials are used is that once they are exposed to radiation, their composition changes in the specific area that was exposed. This thesis utilizes a negative resist, meaning that exposure leads to cross-linking in the polymer chains, making the exposed area harder to dissolve. A positive resist would instead lead to the exposed area being easier to dissolve.

The patterning of the resist happens by scanning the beam in a pattern over it. The exposure of the resist as this happens is, however, a bit more complicated than just drawing a pattern on top of it. The electrons that hit the sample are accelerated with a high energy and therefore penetrate through the resist. Scattering as they interact with its surface. This dilates the beam path, which leads to limitations on the patterning. Details that are smaller than this dilation will be impossible to pattern.

Development is the last stage of the EBL process, for which the sample is submerged in an acid or a base. As the composition of the exposed resist has been altered, it dissolves at a different rate along the patterned region compared to the rest of the resist. Since this thesis utilizes a negative resist it allows for all unexposed resist to be dissolved, by removing the sample from the base after an appropriate time has passed.

2.1.2 Iductively Coupled Plasma--Reactive Ion Etching

Inductively Coupled Plasma Reactive Ion Etching (ICP-RIE) is a method of etching away material from a sample, and it is the main method of etching used in this project. It is a process of etching that utilizes a combination of effects, both physical and chemical to remove material from the surface of a sample [9][10][11].

The etching process starts with the generation of a plasma inside the device chamber. This chamber holds the sample that is to be etched. Before the process, the chamber is pumped and then filled with a gas. A radio frequency passes through a coil which is wrapped around the chamber, creating an oscillating magnetic field inside the chamber. This magnetic field induces an electric field in the gas, transforming it into an inductively generated plasma [12]. The power of the radio frequency that passes through this coil and generates the plasma is called the inductively coupled plasma power, or ICP Power. A simple schematic of the ICP-RIE tool can be seen in figure 3.

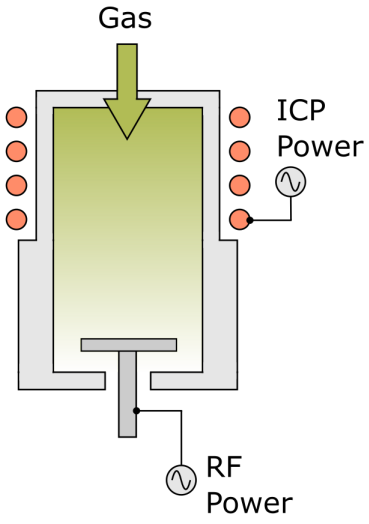

Figure 3: Schematic of a ICP-RIE tool [11].

The radio frequency power source that is marked as RF power is a second power source, different from the one generating the plasma. This power source generates a bias in the sample holder, controlling the flux of ions from the plasma to the sample [13]. As the energized ions in the plasma are accelerated towards the sample they collide with it. The high energy collisions lead to surface material being sputtered away. This is the physical component of the etching process [9].

The chemical component of the process involves reactions between the sample surface and the ions in the plasma. It is therefore dependent on the composition of reactants in this plasma. The process examined in this thesis utilizes a BCl_3/Cl_2 gas to generate the plasma together with a crystalline GaN layer stack on a SiC sample. As the gases ionize and turn into a plasma, the Cl^+, Cl^{2+}, and BCl^{2+} ions dissociate from the precursors. These ions are the ones active in chemical reactions during etching, binding to surface atoms in the sample. These surface atoms then dissociate from the sample [9].

2.1.3 Chemical Wet Etching

Chemical wet etching is a process, widely used in the field of semiconductor processing. The process is utilized for etching but also with the purpose of lapping and polishing a surface. Meaning that it etches down roughness for an optically flat surface, clean and free from damage [14].

The process is described as chemical wet etching simply because it describes how a sample is etched via the process of chemical reactions with a liquid chemical etching solution. The sample that is etched is first saturated with the liquid chemical, often via a process known as immersion etching. This refers to a process

where the sample is immersed in the liquid etching solution. As the sample is saturated with the etching solution, the chemical part of the etching begins. The chemical mechanism of the etching process involves three steps. First, the reactants in the sample diffuse to the surface that's reacting. Here the reactants and the etching solution then undergo a chemical reaction. The products from this reaction are then finally removed from the surface via diffusion into the solution. Uniformity of the etching of the sample is dictated by the etch rate, how much of the sample is removed by the process per unit of time. This etch rate is in and of itself influenced, not only by the quality and quantity of the elements involved but also by the temperature and agitation of the sample during the process. Often some agitation is needed for a uniform etch to be possible [15].

To understand the chemical etching process of GaN we have to start with its atomic structure. GaN has a Wurtzite structure, with a hexagonal unit cell composed of an even number of Gallium and Nitrogen atoms. Each Ga atom bonded to four N atoms, each of those bonded to four Ga atoms. In figure 4 a schematic of this atomic arrangement can be seen [4]. This structure will become relevant when discussing the etching process. In simple terms, the etching is composed of two steps. A reaction between the GaN crystal and the etchant resulting in the formation of oxide, and the later dissolution of that oxide [16]. The etchant is the chemical known as TMAH, or tetramethylammonium hydroxide, which is a non-metallic source for a hydroxide ion. It is utilized as a base and a catalyst.

There is currently a discussion in the field about the precise process of etching, particularly about the oxide formation. The explanation that is predicated upon oxidation with an intermediate step in the etching process, describing the formation of Gallium hydroxide, gives the best description of the directional dependence of the etching. Therefore it is the one presented here.

When a GaN crystal is submerged in TMAH the hydroxide ions are absorbed to its surface, forming Gallium oxide. A proposed chemical reaction for this can be seen below in equation 6, following the intermediate step in equation 7. [16]

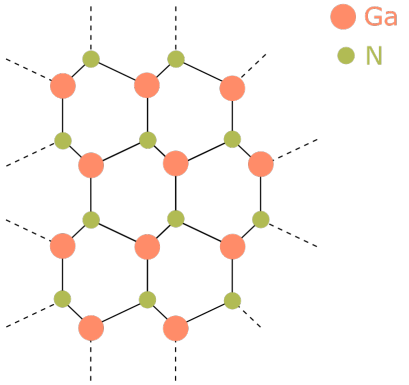

Figure 4: Atomic structure of Ga and N in a Gallium Nitride crystal [4].

$$2GaN + 3H_2O \xrightarrow{TMAH} Ga_2O_3 + 2NH_3 \tag{6}$$

$$GaN + 3H_2O \xrightarrow{TMAH} Ga(OH)_3 + NH_3 \tag{7}$$

These reactions lead to a cyclic process in which exposed Gallium on the sample surface is oxidized, which allows it to dissolve and disappear from the surface. This results in new Gallium being exposed, allowing that to be oxidized, and so on. The steps of this process are outlined in figure 5 below.

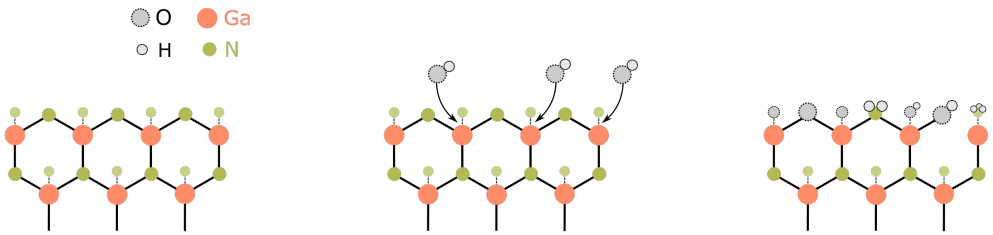

(a) (b) (c)

Figure 5: Step-by-step operation of oxidation of Gallium during chemical wet etching in the direction of the $(1\bar{1}00)$ plane. (a) "Base state" of GaN, before any interaction with the etchant. (b) OH^- ions from the etchant attack the outer Ga-N bonds. (c) OH^- ions from the etchant trigger an oxidation of the outer, now exposed Gallium in the sample. After step (c) the Gallium oxide and hydroxide dissolves, cycling the process back to step (a). But now a layer of atoms deeper in the sample [16].

As this process is predicated upon the reaction between hydroxide ions and Gallium, the structure of GaN now becomes important. After all, the crystal structure determines how the surfaces of the crystal looks, in terms of determining the availability of exposed Gallium for the TMAH solution. Because of this crystal structure, the crystal direction of a sample surface will influence the chemical etching rate [14]. The two directions in the lattice that are of most interest are $<11\bar{2}0>$ and $<1\bar{1}00>$, as they show the most extreme directional dependence. With the etching of GaN being focused almost entirely in the $(1\bar{1}00)$ plane and basically none in the other. In figure 6 the two planes that correspond to these distances are shown in the wurtzite unit cell.

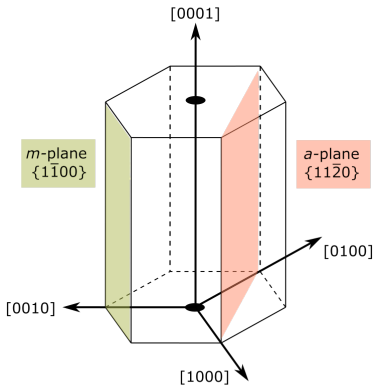

Figure 6: Schematic of a GaN unit cell, <11$\bar{2}$0> and <1$\bar{1}$00> planes marked [17].

As TMAH etches the crystal from different directions, it will encounter different arrangements of atoms. In the direction of the (11$\bar{2}$0) plane, the OH^- ions of TMAH will first reach a surface of Gallium which is oxidized and dissolved [16]. The next layer of atoms from that direction is a layer of Nitrogen dangling bonds. This hinders further progress for OH^- ions, safeguarding the Gallium beneath it and thus halting the etching [16]. If the TMAH instead approaches towards the (1$\bar{1}$00) plane the process turns out differently. Here Gallium is never as far from a newly etched out surface of Nitrogen, allowing for the continuation of the etching process after the first Gallium atoms are oxidized and dissolved.

2.2 Sample Characterization

This section will explore the method that is used for the characterization of samples. This characterization is done by imaging the previously fabricated samples.

2.2.1 Scanning Electron Microscopy

Most of this section is based on the chapter on scanning electron microscopy by Yimei Zhu and Hiromi Inada, from the book "Encyclopedia of Nanotechnology" [18]. Scanning electron microscopy (SEM) is a method for acquiring high-resolution images with features on the nano-scale. Just as the name implies this method involves scanning the sample with a beam of electrons, not entirely different from the one discussed in section 2.1.1 on the EBL. A gun generates a beam of electrons that passes through a system of lenses and apertures before it collides with the sample. Here the beam is scattered by differing elements and features of the samples, detectors then allow for an image to be generated.

The signals that are detected result from electrons that have in some way scattered of the sample. The way this scattering occurs influences the type and property of the signals and therefore also how they are detected. Allowing for characterization and image creation. There are a few different ways that electrons scatter, resulting in different types of signals to detect. There are backscattered electrons, which are generated upon contact with the sample surface. The nuclei of atoms are positively charged, meaning that they attract electrons. This changes the trajectory of electrons in the beam that passes by them. Some electrons will change direction by this method, scattering backward. These electrons are only generated in the very top of the sample surface and therefore give images with a high resolution. Another type of signal are the secondary electrons. These are generated as the highly energized electrons of the beam collide with atoms in the sample. This results in those atoms ionizing as their electrons are knocked away in an inelastic scattering event. Secondary electrons are generated directly as the beam collides with the sample, these are termed SE1. Secondary electrons are also generated deeper in the sample. The high energy of the beam means that it penetrates into the sample. As the beam scatters deeper in the sample, electrons generated from these scattering events will not exit the sample. Instead, they will collide with and ionize other atoms, which results in secondary electrons being generated. This continues until the electrons lose all their energy to collisions or escape the sample. Secondary electrons generated this way and escape the sample are termed SE2. SE2 signals make up the majority of secondary electrons and they are used for the imaging in this thesis. These electrons are generated from a larger area in the sample, leading to a lower resolution but

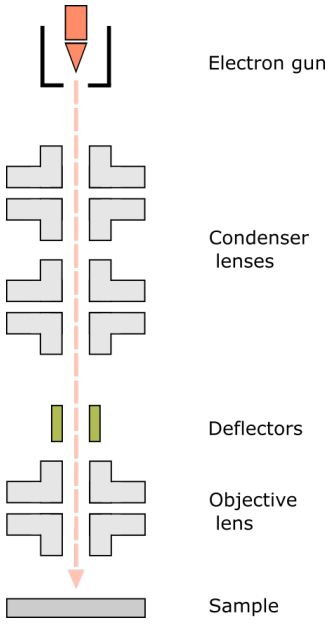

Figure 7: Schematic of a typical SEM system [18].

higher edge contrast compared to images from backscattered electrons. Finally, there are also x-ray signals generated by the electron beam. As the beam collides with atoms it can result in these atoms exiting instead of ionizing. As an exited atom then relaxes it releases a photon which can be detected.

X-rays are detected by photodetectors placed in the chamber holding the sample. Electron signals are detected with scintillators. A scintillator is a material that emits light when excited by ionizing radiation. The electron detectors consist of a positively charged scintillator, attracting the electrons scattered from the sample. As the electrons hit the scintillator light is generated which can be generated into electrical signals with a photodetector. Backscattered electrons are detected by detectors placed directly above the sample, and secondary electrons by detectors placed all around it.

The SEM system can also be used for milling away material from a sample with the application of a focused ion beam (FIB). The FIB system utilizes the SEM system, but ions are accelerated into a beam instead of electrons. As this beam collides with the sample, it sputters away atoms from its surface. As this milling process is done with a focused beam of ions it removes material along a pattern of very high resolution. Allowing for the creation of a detailed cross-section that can be observed with the SEM.

3 Method

In this section, the experimental process for the sample fabrication will be presented. The steps in this process will be described and the reason behind them explained.

3.1 The GaN Fin Fabrication Process

The process carried out for this thesis can be divided into 7 distinct steps which will be discussed in this section. Furthermore, SEM is used to inspect samples in-between steps and after the process. A general outline for this process can be seen in table 1. An expanded version of this table can be seen in appendix A. In figure 9 A schematic of the sample during these steps can be seen. The process is carried out on a base sample consisting of a GaN stack on top of a SiC substrate. The GaN stack is composed of differently doped layers: a 100nm n+ doped GaN layer, on top of a 2μm n- doped GaN layer, on top of a 500nm n+ GaN layer, on top of a 100nm layer of unintentionally doped GaN (UID-GaN). This stack is placed on top of a 50nm AlN buffer layer before the SiC substrate. This GaN stack was fabricated by a group in Linköping. A schematic of this stack can be seen in figure 8.

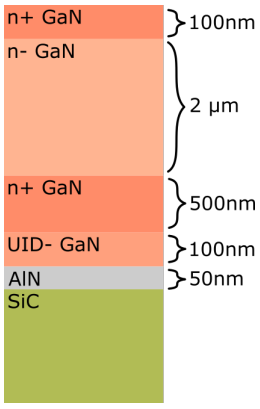

Figure 8: Schematic of the GaN layer stack that compose the base sample.

Table 1: Sample fabrication steps.

Step	Short description
Cleaning	Organic impurities removed from sample
Resist spin-on	Resist applied to sample
Pattern lithography	Sample patterned with EBL
Development	Pattern developed with TMAH
Dry etch	Sample etched with ICP-RIE
Wet etch	Sample etched with TMAH

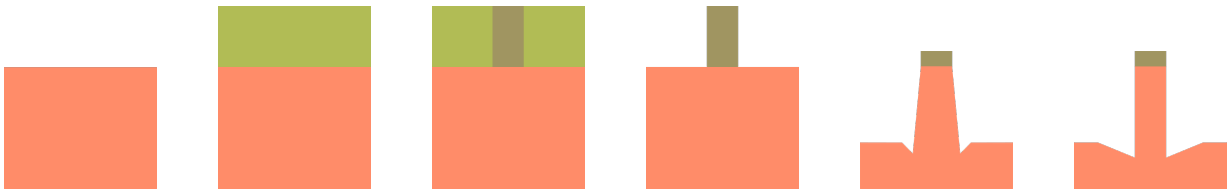

(a) Cleaned sample (b) Resist applied (c) Resist patterned (d) Resist developed (e) Dry etch (f) Wet etch

Figure 9: Schematic of the fabrication process, along the steps described in table 1. Dimensions of fin sidewall slope and trenches that can be seen in figure (e) and (f) are exaggerated.

3.2 Etching Preparatory Steps

The first step of the process is removing any organic impurities from its surface with a cleaning step. The sample is submerged in a beaker with Acetone which is placed in an ultrasonic bath for 2 minutes. The sample is then submerged in a beaker with IPA which is also placed in an ultrasonic bath for 2 minutes. After which it is placed on a 100°C hot plate for 2 minutes. The sample is then placed in a plasma asher. This device uses an oxygen plasma to vaporize organics on the sample which are then pumped away.

The next step is the resist spin-on. In this step, the resist is applied to the sample with a spin coating method. First, the adhesion promoter SurPass 3000 is applied to the sample with a spin coating recipe of 3000 rpm for 30 seconds. This promotes an easier adhesion of the resist on the sample. The sample is then washed in de-ionized water (DIW). Before the resist is applied on the sample it is baked at 200°C for 3 minutes, to remove solvents and also promote adhesion. This is called a dehydration bake. The negative resist used is a hydrogen silsesquioxane (HSQ). In this thesis, the specific HSQ used is FOX15. This is applied with the spin coating recipe of 6000 rpm for 45 seconds. After the resist is spun on the sample is baked at 200°C for 2 minutes, to harden the resist.

The sample is then patterned in the EBL with a pre-programmed pattern. This pattern consists of a grid of fin arrays. In each array there are 10 fins of a certain width, at certain consistent distances. Varying along the rows and columns of the grid, see figure 10. Patterning the sample this way allows for examination of which fin sizes can be etched, and how close to each other these fins can be placed.

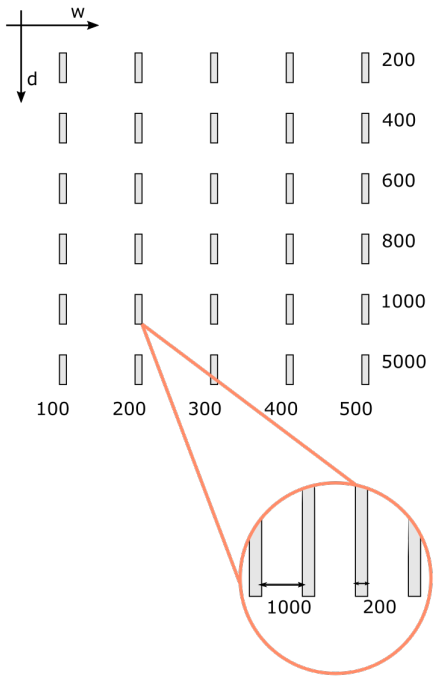

Figure 10: Schematic of fin grid pattern. The width (w) of the fins increase along the w-direction. The steps of the width are marked along this direction in nm. The distance (d) between fins increase along the d-direction. The steps of the distance are marked along this direction in nm. Enhanced area shows a schematic of the fin array at the w = 200 nm and d = 1000 nm array.

After the patterning, the sample is developed. The sample is submerged during agitation first into a solution of 25% TMAH for 1 minute, then DIW for 1 minute, and finally IPA for 1 minute. The TMAH in the solution will dissolve the unpatterned resist, leaving only the grid of fin arrays. The DIW and IPA will wash away byproducts from the dissolving resist as well as remaining TMAH, stopping further development of the sample as well as keeping it clean.

3.3 Dry Etching Step

The next step is the main one of interest for this thesis, the dry etch. This is done with the ICP-RIE, which allows for the variation of parameters during the process. This varying of parameters is supposed to influence the shape of the resulting fins.

Three series of samples were dry etched, with different parameters being varied each time. These are RF power, ICP power, and BCl_3/Cl_2 gas ratio. The etch time has also been varied in an attempt to etch fins with a height of 1μm. In total, 13 samples were dry etched for this thesis. All these dry etched samples and their respective variable parameters are presented in table 2.

Table 2: All dry etched samples, with their respective RF and ICP powers, BCl_3 gas ratios and etching times.

Series #	Sample #	RF Power [W]	ICP Power [W]	BCl_3 ratio [%]	Etch time [min]
1	1	40	300	10	2.5
1	2	40	600	10	2.5
1	3	80	300	10	2.5
1	4	80	600	10	2.5
2	1	80	300	10	1.4
2	2	40	600	10	1.9
2	3	120	300	10	1
2	4	120	300	40	1
2	5	120	300	30	1
2	6	120	300	20	1
3	1	120	300	10	1.2
3	2	120	300	20	1.7
3	3	120	300	30	1.4

3.4 Wet Etch

The final step in the process is the wet etch. Here the samples are submerged into beakers of TMAH. Samples in series 1 and 2 are then subsequently heated up to 40°C. Samples in series 3 were submerged into beakers of TMAH which are already heated to 40°C. The samples are then left in the TMAH for differing amounts of time. Some samples are etched for a single longer time. Other in multiple shorter time intervals, restarting the process each interval. This etch is supposed to finalize the fins, giving them smooth sidewalls.

In total, 10 samples were wet etched. All these samples and their respective etch times are presented in table 3.

Table 3: All wet etched samples, with their respective etching time intervals and total etching times.

Series #	Sample #	Interval etch times [min]	Total etch time [min]
1	1	30	30
2	1	20 + 30	50
2	2	20 + 10	30
2	3	20 + 10	30
2	4	30 + 10 + 10	50
2	5	30 + 10 + 10	50
2	6	30 + 10 + 10	50
3	1	40	40
3	2	30	30
3	3	20	20

3.5 Trench Imaging

Cross-sections of fins were created in order to acquire better images of the trenches, allowing them to be measured and analysed. The creation of these cross-sections was attempted with two different methods. The first method for this was simply breaking the sample in two, by hand. For this method to work, the break needs to hit directly through a fin array. This was facilitated by adding an array of fins, with about the length of the entire fin grid pattern, during the fabrication. The length of this array would ensure that breaking the sample in two would break that array in two as well. This array of long fins was added to the second and third series of samples.

The FIB functionality of the SEM system can also be used to create cross-sections. First Platinum is deposited over the array of interest in to protect the fin architecture. The ion beam, accelerated with a higher voltage is used to mill away material in that array. This creates a hole in the sample with its edge showing a cross-section of the fins in the array it is created at. The higher acceleration voltage makes the process faster, but the beam more unstable. A lower acceleration voltage is then used to mill the final edge of this hole. The lower voltage increases the resolution of the FIB functionality. The high resolution of the FIB functionality means that it can create very sharp edges. Allowing for the reliable creation of cross-sections of high quality.

4 Results and Discussion

In this section, the results from the fabrication will be presented. This will include SEM images of samples and graphs created with measurements from these images. These will be measurements of etch rates as well as fin sidewall slopes. An exaggerated schematic, showing how this slope is measured is shown in figure 11. By the nature of this calculation, as the fin sidewalls are not perfectly straight as this schematic, the slope measurement is not very precise. Therefore the exact numerical values of slope measurements are not too important. Trends in the change of slopes will instead be looked at. The results of a simulation of the electric field through a fin will also be presented. These results will be compared to and analyzed in relation to earlier presented theory and literature.

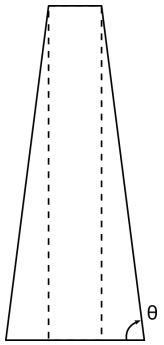

Figure 11: Schematic of angle θ that is measured as fin sidewall slope. Dotted line shows perfectly straight sidewalls.

4.1 Dry Etch

In this section, the results from the dry etch will be explored. The dry etched samples will have RF power, ICP power, and BCl_3/Cl_2 gas ratio varied from an original recipe. This original recipe consists of an RF power of 40 W, an ICP power of 300 W, and a BCl_3 ratio of 10%. Images of dry etched samples will be presented and analyzed according to the literature.

Tilted side view images of the fins in this section are from samples that are etched for differing amounts of times, meaning that fin height is not an accurate measurement of etch rate by itself. Instead it has to be calculated by dividing the fin height by the etch time.

4.1.1 Power Variations

To investigate the effect of the RF and ICP powers on the etching process, all other parameters in the ICP-RIE were kept constant as these two were increased. They were increased from a starting value of 40 W RF power and 300 W ICP power, at a BCl_3 concentration of 10%. Figures 12 and 13 show fins with the same patterned width and distance between them, as the RF power is increased from the original 40 W to first 80 W and then to 120 W.

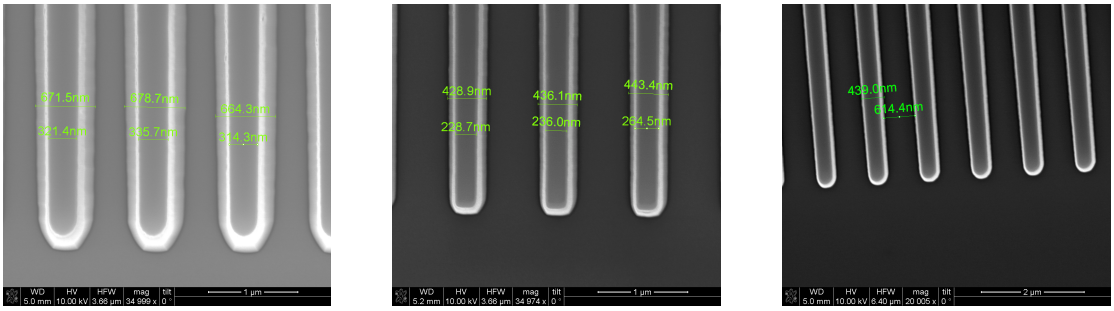

(a) 40 W RF, Etched 2.5 minutes

(b) 80 W RF, Etched 1.4 minutes

(c) 120 W RF, Etched 1 minute

Figure 12: Top view of fins patterned with the same width and distance between them, etched with varying RF power. ICP power and BCl_3 concentration kept constant at 300 W and 10%, respectively. Figure (a) shows fins etched with a RF power of 40 W, figure (b) shows fins etched with a RF power of 80 W and figure (c) shows fins etched with a RF power of 120 W.

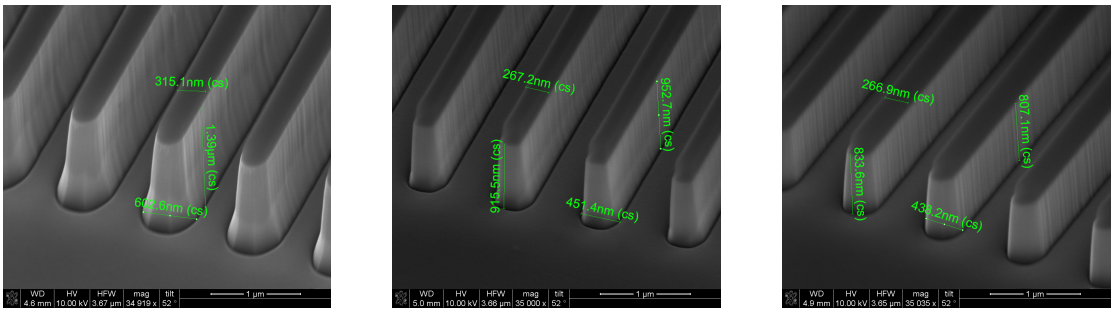

(a) 40 W RF, Etched 2.5 minutes

(b) 80 W RF, Etched 1.4 minutes

(c) 120 W RF, Etched 1 minute

Figure 13: Tilted side view of fins patterned with the same width and distance between them, etched with varying RF power. ICP power and BCl_3 concentration kept constant at 300 W and 10%, respectively. Figure (a) shows fins etched with a RF power of 40 W, figure (b) shows fins etched with a RF power of 80 W and figure (c) shows fins etched with a RF power of 120 W.

In figure 12 the shape of the fins can be seen changing with an increasing RF power. They seem to grow more straight and even. A further investigation into a tilted side view of the fins is shown in figure 13. The dark area on top of the fins is resist left over from the patterning. The fins slope outwards in an outskirting before the sample surface. Around the fins, at the sample surface a small dark region can be seen, this is the trench. It is also worth noting the cleanliness of the sample surface. No impurities of any kind can be seen. This is a good result as it means that the etching process does not contaminate the samples. Figure 13 shows the height of the fins changing with the increasing RF power, increasing the etch rate from the original recipe shown in figure (a). However, not only the rate varies with the RF power. Even the outskirting gets less pronounced as the RF power is increased, it has disappeared from the fins in figure 13 (c). Intending to optimize the etching process, this is a good result because the straight and smooth shape allows for easier fabrication further along in the transistor fabrication process. Smoother walls aid in making sure the wet etch process is carried out consistently. Meaning that it will not start to etch away and destroy the fins from the sidewalls. Smooth walls prevent this as the wet etch needs a rough facet to start etching, it can not start etching straight into a smooth sidewall.

Increasing the RF power enhances both the chemical and physical components of the etching process. It does this via a strong correlation to the bias underneath the sample [9][19][13]. As this bias increases, it raises the energy of the active ions [13]. With this energy increase, the sputtering of the sample is strengthened, increasing the physical etch rate. The increased sputtering also affects the etching in other ways than removing more material. It assists with the process of breaking bonds on the sample surface and it also increases the removal of byproducts that form as the sample is etched [19]. This assists the chemical etching process, leading to an increased chemical etching rate as well [19]. The etching results seen in figures 12 and 13 are in accordance with this. The etch rate increasing with the RF power follows the theory, as both components of the etching process are enhanced. The observed stepper sidewalls can also be understood with this knowledge of enhanced etching. The physical component of the etching process is, unlike the chemical component, anisotropic [13]. The ions that sputter the material are attracted from the plasma in a straight direction down towards the sample surface. Therefore any sections of the fin sidewalls that protrude or slope out will etch at a proportionally higher rate than smooth straight sidewalls.

Figures 14 and 15 shows fins with the same patterned width and distance between them, as the ICP power is increased from the original 300 W to 600 W.

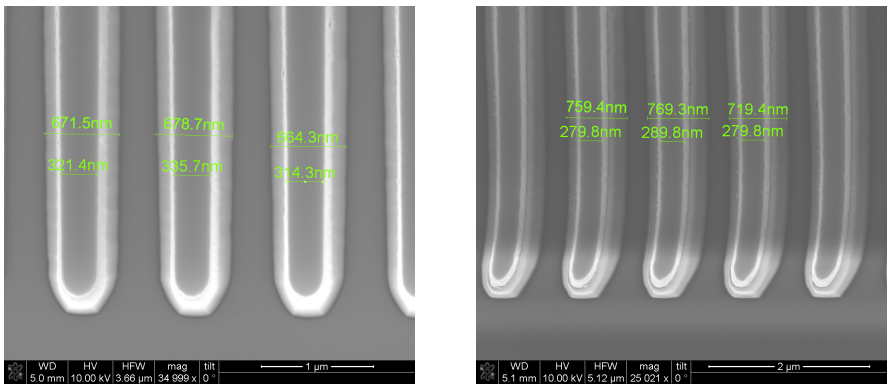

(a) 300 W ICP, Etched 2.5 minutes

(b) 600 W ICP, Etched 2.5 minutes

Figure 14: Top view of fins patterned with the same width and distance between them, etched with varying ICP power. RF power and BCl_3 concentration kept constant at 40 W and 10%, respectively. Figure (a) shows fins etched with a ICP power of 300 W and figure (b) shows fins etched with a ICP power of 600 W. Curvature in image is a distortion from imaging.

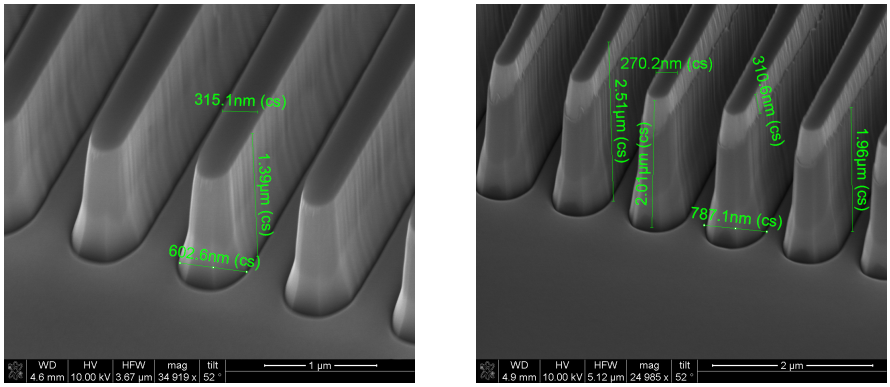

(a) 300 W ICP, Etched 2.5 minutes

(b) 600 W ICP, Etched 2.5 minutes

Figure 15: Tilted side view of fins patterned with the same width and distance between them, etched with varying ICP power. RF power and BCl_3 concentration kept constant at 40 W and 10%, respectively. Figure (a) shows fins etched with a ICP power of 300 W and figure (b) shows fins etched with a ICP power of 600 W.

Figure 14 shows how the shape in contrast to the increase in RF stays consistent for the ICP power increase. A further investigation into a tilted side view of the fins is shown in figure 15. The dark area on top of the fins is resist left over from the patterning. These fins, just as those seen in figure 13, can be seen to slope outwards in an outskirting before the sample surface, where a trench can be seen around them. It is also worth noting the cleanliness of this sample surface as well. No impurities of any kind can be seen. This is a good result as it means that the etching process does not contaminate the samples.

Figure 15 (b) shows that the height of the fins changes with the increasing ICP power, increasing the etch rate from the original recipe shown in figure (a). The high etch rate has resulted in the resist on the side of the fins in figure 15 (b) disappearing and the subsequent etching of the fin tops. This is simply an issue of the etching time being too long considering the etching rate since the etching away at the top of the fin destroys its shape. Disregarding this etching away at the top of the fins, the overall shape of the fins is still unchanged.

ICP power, which generates the plasma, correlates with the etching mainly via its influence on the plasma density [19]. As the ICP power is increased, the density of ion species in the plasma increases as the density of neutral species shrinks [19]. For the BCl_3/Cl_2 plasma, this means an increase in the concentration of the Chlorine ion component. This is the chemically reactive driving force for the etching process so the result will be an increased chemical etching rate [19][13]. However, an increase in the ICP power also results in a decrease in the bias underneath the sample [19]. As this bias is directly correlated to the energy of the ions in the plasma, a decrease in the bias reduces their energy. This results in a weakened sputtering effect, in contrast to the otherwise increased chemical etching rate. The etching results seen in figures 14 and 15 are in accordance with this. An increase in the etching rate follows from an enhanced chemical etching component if the weakening effect on the physical etching component is smaller than this enhancement [19][13]. This can be assumed to be the case since the etch rate increases. As the ICP power is increased, the chemical component of the etching will dominate over the decreasing physical component during the etching process[13]. The chemical etching component consists of chemical reactions between the sample surface and its immediate surroundings, meaning it is isotropic [13]. This explains why the shape of the fins does not change with an increase in ICP power, unlike RF power.

In figure 16 the measurable variations in the etching process, etch rate, and fin sidewall slope, resulting from the RF and ICP power variations are shown. The etch rate for individual samples is calculated by dividing the averaged height of the fins by their respective etching times. Rates for samples with the same variable parameters are then averaged. Fin sidewall slopes are calculated in the same way, with the slope described in figure 11. The etching rate of the GaN fins can be seen increasing with an increase of either RF or ICP power. The increase in RF power leading to a proportionally higher increase in etch rate per watt, compared to ICP power. The slope follows a similar relationship with the etch rate, increasing as the powers increase.

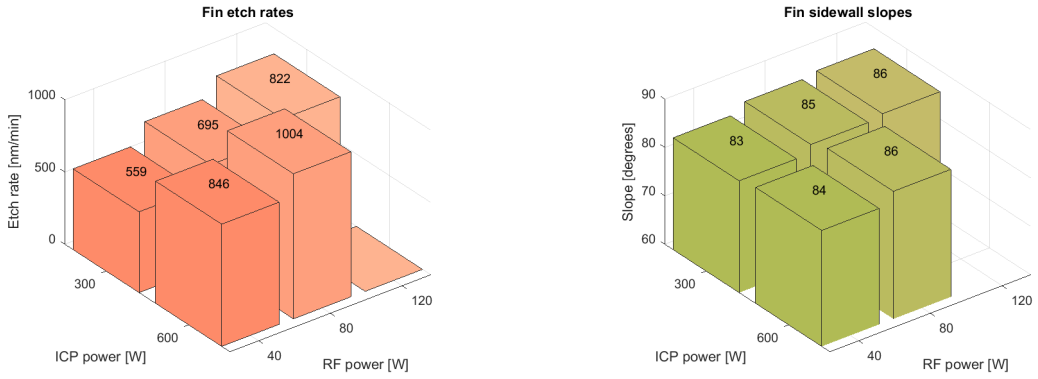

(a) Etch rate averages

(b) Slope averages

Figure 16: Measurable variations in the ICP-RIE etching process, resulting from variations in RF and ICP powers. Composed of measurement values from all series of samples which are normalized against their etching times. Different measurements with the same powers are averaged together. Figure (a) shows the relationship between the RF and ICP powers of the ICP-RIE process, and the etch rate of the GaN fins. Figure (b) shows the relationship between the RF and ICP powers of the ICP-RIE process, and the slope of those fins.

The ICP power can be seen to have a larger influence on the rate than an increase of the RF power, with the highest etching rate achieved with both an increased RF and ICP power. The slope of the fin sidewalls, as seen in figure 16 (b) also changed over both of the power variations. The outskirting of the fins was, however, only removed as the RF power increased, leading to an increased slope. Even as the ICP power has a larger effect on the etch rate. The increase in ICP power also introduced some difficulties for the etching device. Trenches are present around the fins for both the RF and ICP power increase, but with these images, it is not possible to draw any conclusion on the power variations effect on those trenches. This will be explored in section 4.3, further along in the thesis.

4.1.2 Gas Ratio Variations

To investigate the effect of the BCl_3/Cl_2 gas concentration ratio on the etching process, all other parameters in the ICP-RIE were kept constant as the ratio of BCl_3 was increased. The ratio was increased from an original recipe of 10% BCl_3, with an RF power of 120 W and an ICP power of 300 W. Figures 17 and 18 show fins with the same patterned width and distance between them, as the BCl_3 ratio is increased from the original 10% to first 20%, then to 30% and finally to 40%. The ICP-RIE has been cleaned in between each change of the BCl_3 ratio, to ensure the chamber is not contaminated by BCl_3/Cl_2 gas residues.

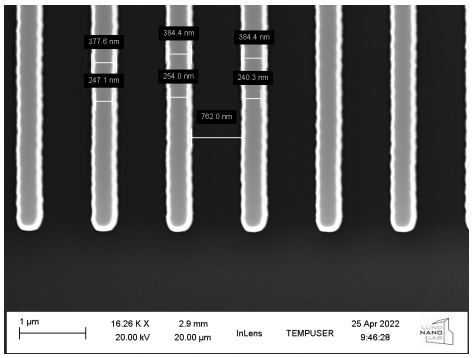

(a) 10% BCl_3,
Etched 1.2 minutes

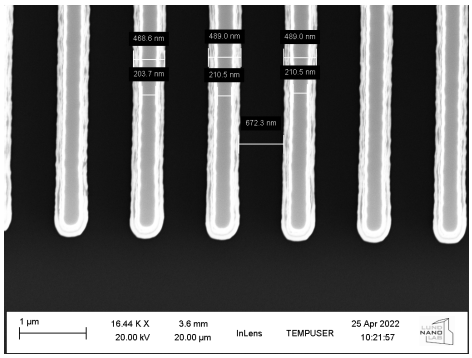

(b) 20% BCl_3,
Etched 1.7 minutes

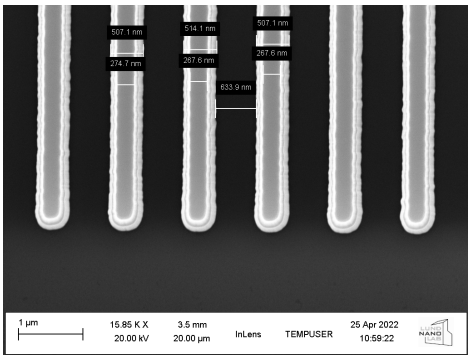

(c) 30% BCl_3,
Etched 1.4 minutes

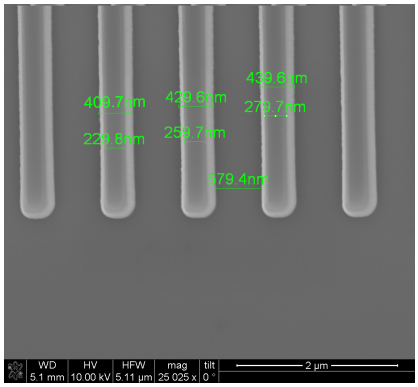

(d) 40% BCl_3,
Etched 1 minute

Figure 17: Top view of fins patterned with the same width and distance between them, etched with varying BCl_3 concentrations. RF and ICP power kept constant at 120 W and 300 W, respectively. Figure (a) shows fins etched with a BCl_3 concentration of 10%, figure (b) shows fins etched with a BCl_3 concentration of 20%, figure (c) shows fins etched with a BCl_3 concentration of 30% and figure (d) shows fins etched with a BCl_3 concentration of 40%.

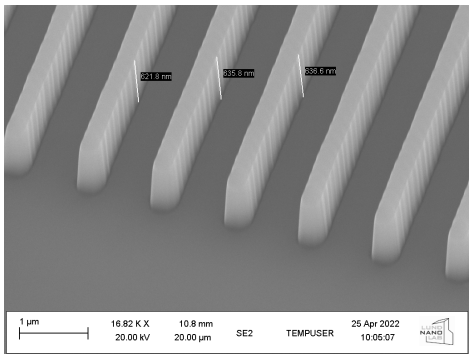

(a) 10% BCl_3,
Etched 1.2 minutes

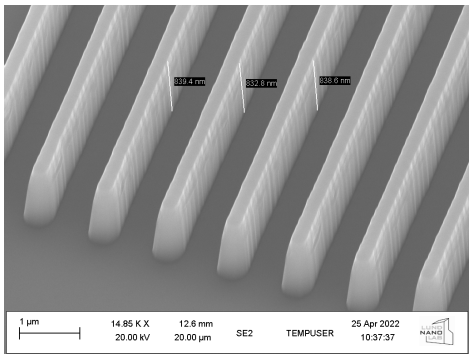

(b) 20% BCl_3,
Etched 1.7 minutes

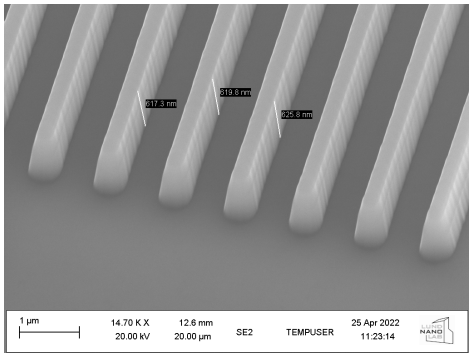

(c) 30% BCl_3,
Etched 1.4 minutes

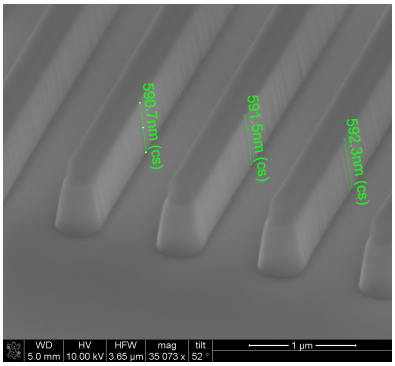

(d) 40% BCl_3,
Etched 1 minute

Figure 18: Tilted side view of fins patterned with the same width and distance between them, etched with varying BCl_3 concentrations. RF and ICP power kept constant at 120 W and 300 W, respectively. Figure (a) shows fins etched with a BCl_3 concentration of 10%, figure (b) shows fins etched with a BCl_3 concentration of 20%, figure (c) shows fins etched with a BCl_3 concentration of 30% and figure (d) shows fins etched with a BCl_3 concentration of 40%. Figures (a), (b) and (c) are taken without internal angle correction, meaning that the numerical values of the height in the image are incorrect. The values are numerically corrected by dividing the height displayed with the sine of the image tilt angle.

Figure 17 shows how the shape of the fins goes unchanged as the BCl_3 gas ratio is increased. A further investigation into a tilted side view of the fins is shown in figure 18. The dark area on top of the fins is resist left over from the patterning. The fins slope outwards in an outskirting before the sample surface, where a trench can be seen around them. It is also worth noting the cleanliness of the sample surface. No impurities of any kind can be seen. This is a good result as it means that the etching process does not contaminate the samples. Figure 18 shows the height of the fins changing with the increasing BCl_3 gas ratio. The slope can be seen to also decrease with the BCl_3 gas ratio.

The etching process of the device is influenced by the environment in the device, not only by the powers that start and drive the etching process. By changing the chemical environment, the chemical etching process

will be changed along with it [9]. The term "chemical environment" refers to the molecules and ions that can be found inside the chamber of the ICP-RIE during the etching process. Changing this environment means changing the ratio of BCl_3/Cl_2 within it. Taking a hypothetical sample with 0% BCl_3 and slowly increasing that percentage will result in the etching rate increasing as well [13][9]. Introducing BCl_3 to the environment results in the presence of the active ions Cl^+ and Cl^{2+}, which drive chemical etching [13]. Increasing the ratio of BCl_3 raises the tendency for these ions further, increasing their density. A larger density of the ions that drive the chemical etching means a higher etch rate [13]. The relationship between the ratio BCl_3/Cl_2 and etch rate is, however, not linear. After BCl_3 reaches 10% a further increase will now instead result in a lowering of the etch rate. Cl^+ and Cl^{2+} ions have at this percentage reached a peak in their density. Adding more BCl_3 beyond this point will just result in the density of BCl^{2+} increasing at the expense of Cl^+ [9]. As the density of active ions decreases, the rate of the chemical etching they drive decreases as well.

In figure 19 the measurable variations in the etching process resulting from this investigation are shown. Etch rates for samples are calculated by dividing the average height of the fins by their respective etching times. Fin sidewall slopes are calculated as described in figure 11.

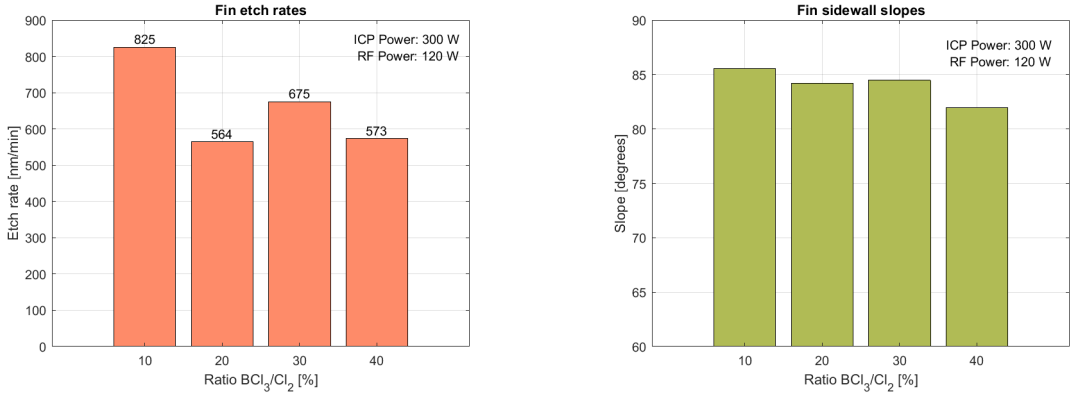

(a) Etch rate averages

(b) Slope averages

Figure 19: Measurable variations in the ICP-RIE etching process, resulting from variations in the BCl_3/Cl_2 gas ratio. Composed of measurement values from the second series of samples, normalized against their etching time. Taken without cleaning the etcher in between gas ratio changes. Figure (a) shows the relationship between the BCl_3/Cl_2 gas ratio during the ICP-RIE process and the etch rate of the GaN fins. Figure (b) shows the relationship between the BCl_3/Cl_2 gas ratio during the ICP-RIE process and the fin sidewall slopes.

The etching rate of the GaN fins can be seen initially decreasing with an increased BCl_3/Cl_2 gas ratio. After this initial decrease, the relationship takes an unexpected shape. Instead of continually decreasing like the literature would suggest it first increases before returning to the previous value. The slope follows a similar relationship to the etch rate as the ratio is increased. These measurements are however taken without cleaning the ICP-RIE in between each sample, starting with the 40% BCl_3 ratio, then 30, then 20 (the sample with a 10% BCl_3 ratio was taken at an earlier time). It is possible that without cleaning the chamber of the ICP-RIE the process becomes contaminated with traces of BCl_3. This change in environment would affect the etching process. In figure 20 the measurements are taken as the ICP-RIE is cleaned in between

each sample (the sample with a 10% BCl_3 ratio was taken at a earlier time). Etch rates for samples are calculated by dividing the average height of the fins with their respective etching times. Fin sidewall slopes are calculated as described in figure 11.

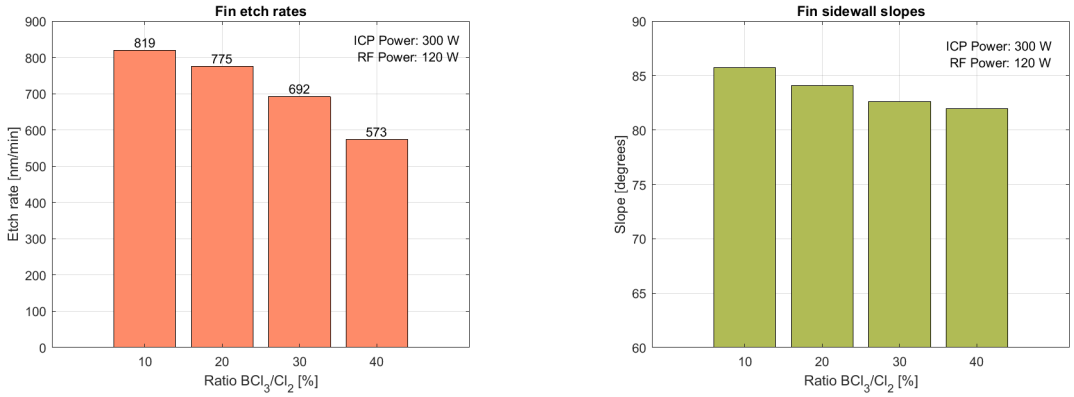

(a) Etch rate averages

(b) Slope averages

Figure 20: Measurable variations in the ICP-RIE etching process, resulting from variations in the BCl_3/Cl_2 gas ratio. Composed of measurement values from the second series of samples, normalized against their etching time. Etcher has been cleaned in between gas ratio changes. Figure (a) shows the relationship between the BCl_3/Cl_2 gas ratio during the ICP-RIE process and the etch rate of the GaN fins. Figure (b) shows the relationship between the BCl_3/Cl_2 gas ratio during the ICP-RIE process and the fin sidewall slopes.

Here the etch rate of the fins decreases continuously as the BCl_3 ratio is increased. The fin sidewall slope follows as similar relationship to the etch rate as the ratio is increased here as well. In accordance with literature and unlike the results shown in figure 19. Ensuring that the chamber was not contaminated by BCl_3/Cl_2 gas residues changed the resulting etch rates to align with whats postulated by the literature on the subject [13]. Seemingly confirming that subsequent BCl_3/Cl_2 gas ratio measurements contaminate the etching process. The images shown earlier in figures 17 and 18 are from measurements where the chamber has been cleaned in between BCl_3/Cl_2 gas ratio variations to prevent this contamination. As the BCl_3 ratio increase results in a lower etch rate and higher slope, it gives the impression that increasing the ratio is a negative change for the etching process. It would be negative since the wanted result is straight and smooth sidewalls. The reason that increasing the BCl_3 ratio could be worthwhile is that it should reduce the trenches as well. According to Yue et al. [13], an increase in the BCl_3 ratio to 40% should result in the trenches disappearing. A result that strongly differs from the one presented in figure 18 (d), where these trenches can still be seen clearly. The removal of the trenches after the dry etch would result in the wider trenches, also called grooves, not forming after the wet etch. They form when the TMAH start to etch away the sample from the already existing trenches, as their rough surface gives the TMAH an area to start etching. Preventing the trenches from forming during the dry etch would therefore prevent the grooves from forming.

4.2 Wet Etch

In this section, the results from the wet etch will be explored. The wet etched samples will have etching times varied from an original recipe of 20 minutes. Images of wet etched samples will be presented and analyzed according to the literature.

In figure 21 the top view of fins patterned with the same width and distance between them, etched in multiple intervals of varied times is shown. Figure 22 Shows fins etched with varying times but in a single interval of time.

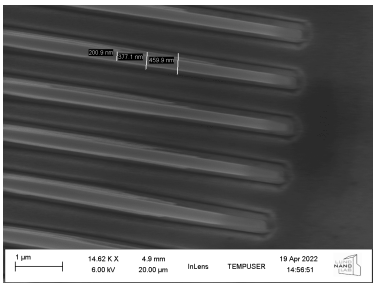

(a) 20 + 30 minutes

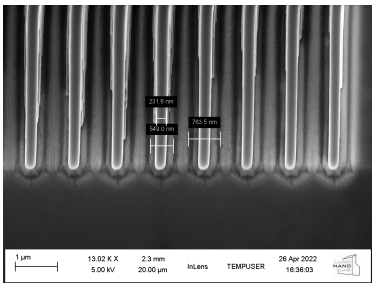

(b) 20 + 10 minutes

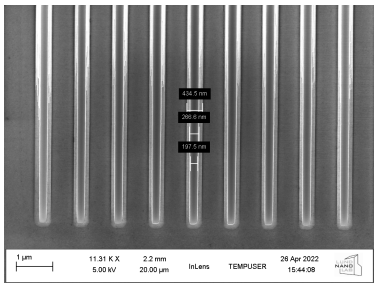

(c) 30 + 10 + 10 minutes

Figure 21: Top view of fins patterned with the same width and distance between them, wet etched with varying times, in multiple batches. Figure (a) shows the first sample of the second series, etched for a total of 50 minutes in two batches. Figure (b) shows the second sample of the second series, etched for a total of 30 minutes in two batches. Figure (c) shows the fourth sample of the second series, etched for a total of 50 minutes in three batches.

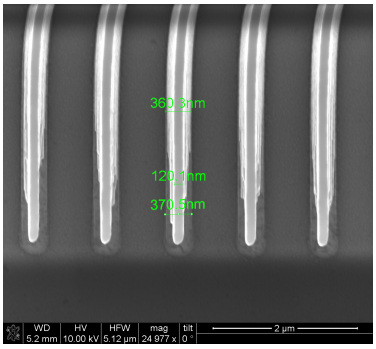

(a) 20 minutes

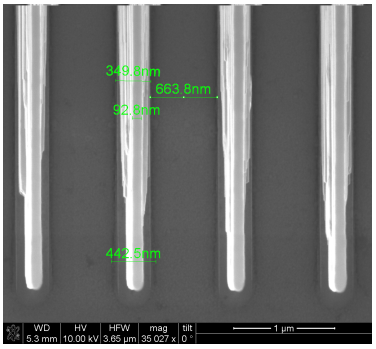

(b) 30 minutes

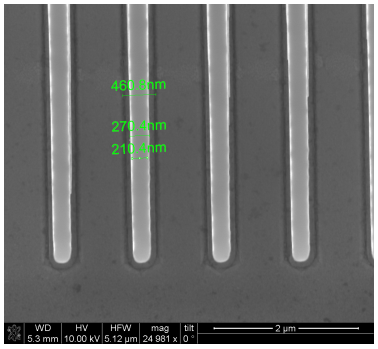

(c) 40 minutes

Figure 22: Top view of fins patterned with the same width and distance between them, wet etched with varying times. Figure (a) shows the third sample of the third series, etched for 20 minutes. Figure (b) shows the second sample of the third series, etched for 30 minutes. Figure (c) shows the first sample of the third series, etched for 40 minutes.

The images in figures 21 and 22 show that most wet etching recipes did not result in a complete wet etch. A complete wet etch would be a wet etch process that results in smooth sidewalls along the entire fin array. A few microns from the tip of the fins, a surface of facets can be seen. This leads to the assumption that the wet etch process is not completed. This assumption is confirmed by looking at the width of the thinner section of the fins. This section has the actual width that was patterned. Meaning that the facets still need to be etched away to achieve a smooth sidewall.

Figure 21 shows fins wet etched in multiple smaller intervals of time. Even though the final etching time is higher than for some of the other samples, the wet etch is still not complete. The process for etching these samples included submerging the samples in TMAH and then subsequently heating them. Meaning that the heating of the solution is part of the etching time. There may be some sort of ramp-up time for the etching process with this method, which most probably has a slower etch rate due to the lower temperature. It needs to be investigated further. Figure 22 shows samples heated for a single longer period, in TMAH heated to 40°C. Figure 22 (c) seems to show a complete wet etch. A further investigation of sample 22 (c) is shown in figure 23. A further investigation, in this case, entails a tilted side view image of the fins and a top view image from the center of the fin array.

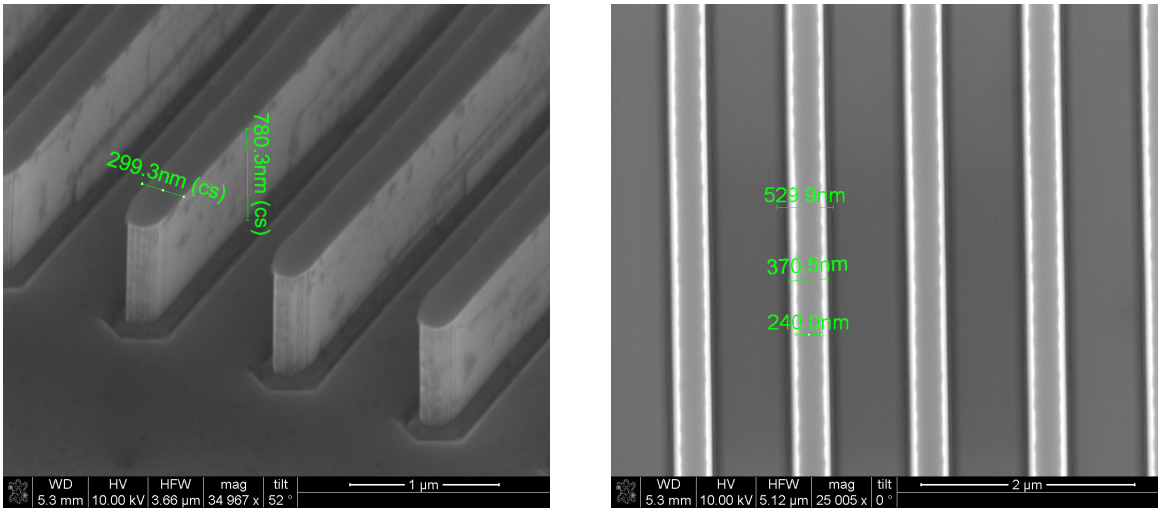

(a) Tilted side view

(b) Top view in middle of fin array

Figure 23: Further images of the first sample in the third series, wet etched for 40 minutes in a singular batch. Figure (a) shows a tilted side view of the fins and figure (b) shows a top view from the center of the array of fins.

Figure 23 (a) shows that the sidewalls are not smooth. Some facets can be seen along them. Grooves around the fins can also be seen in this figure. As mentioned in section 4.2, these grooves form as the trenches are exposed to the wet etch process. The TMAH uses the rough facets in trenches to start etching away at the sample. Figure 23 (b) shows the middle of the fin array. The wet etch progress from the tip of the fins, meaning that this area will be wet etched last. The brighter regions at the edge of the fins in this figure are the sloped sidewalls that skirt out. Their presence means that the wet is still not entirely complete. These regions are however very thin compared to the same regions on the other fins in figures 21 and 22. This

means that the wet etch process is almost complete. Increasing the wet etch time by 10 minutes, to a total of 50 minutes, should result in a complete wet etch.

The grooves that form around the fins during the wet etch process should be reduced in size or removed to optimize the etching process. An optimized etching process would result in a sample with straight fins with smooth sidewalls and no etching on the sample surface. The wet etch of the sidewalls can be completed by increasing the etching time slightly, but to prevent the grooves from forming the trenches need to be prevented from forming.

4.3 Trench Measurements

In this section, the results from trench measurements will be explored. Trenches are measured from cross-sections created at the tip of the fins with the FIB functionality of the SEM. Images of trench cross-sections will be presented and analyzed according to the literature.

The FIB functionality of the SEM system has been used to generate cross-sections of certain fins. In some cases, this allowed for the trenches around the fins to be measured, as shown in figure 25. Details in the images were to small too measure in the SEM system but they have been measured afterward. Figure 24 shows cross-sections where the size of the trenches could not be measured effectively.

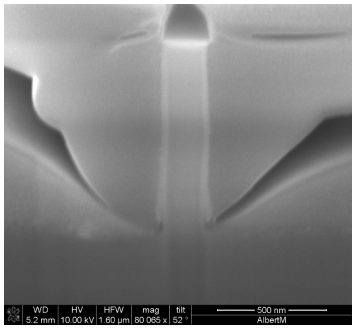

(a) 40 W RF power,
Wet etched 30 minutes

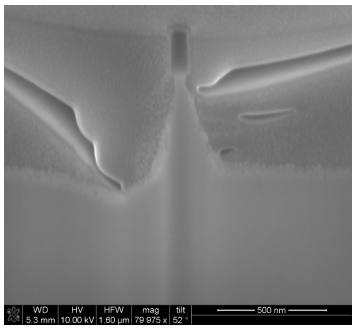

(b) 120 W RF power,
40% BCl_3

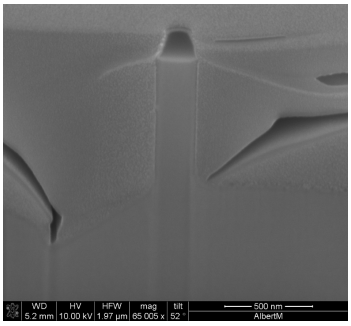

(c) 120 W RF power,
Wet etched 40 minutes

Figure 24: Cross sections of fins after FIB process. Figure (a) shows sample one of the first series, after the wet etch step. Figure (b) shows sample four of the second series, after the dry etch step. Figure (c) shows sample one of the third series, after the wet etch step. See table 3 for details about the fabrication of the samples in (a) and (c). See table 2 for details about the fabrication of the sample in (b).

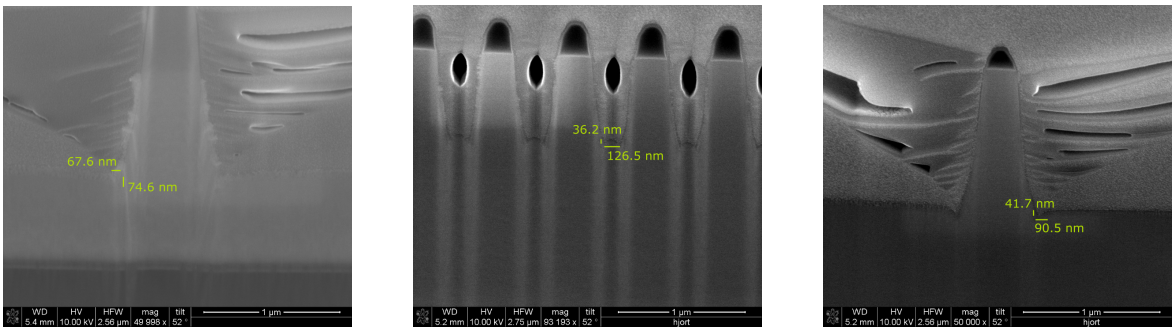

(a) 40 W RF power (b) 80 W RF power (c) 120 W RF power

Figure 25: Cross sectional images of fins after FIB process with manual measurements. Figure (a) shows FIB cross section of sample two of the first series, after the dry etch step. Figure (b) shows FIB cross section of sample one of the second series, after the dry etch step. Figure (c) shows FIB cross section of sample three of the second series, after the dry etch step. See table 2 for details about the fabrication of these samples. Measurements have been placed on figures after the imaging process.

Figures 24 and 25 shows cross-sectional images, fabricated and wet etched under varying conditions. The area at the bottom of the images is the base of the sample and the pillar (multiple pillars in figure 25(b)) sticking out upwards from it are the fins. These areas have a different brightness than the area around them, in the rest of the image. This surrounding area consists of platinum, deposited to protect the structure during the FIB process. The Dark spots at the top of the fins are resist left over from the fabrication process. Dark spots at the side of the fins are voids in the deposited platinum.

Figure 24 shows images of samples where the trench size can not be measured. Figure (a) shows a wet etched sample where the groove size cannot be distinguished. This fin is seen to have smooth sidewalls, the distortion in the middle of the fin is from the imaging of it. Considering the size of the image, the grooves that form during the wet etch should be visible in this image. The figures in section 4.2 show that the grooves should be smaller than the dimensions of this image. For some reason, however, they can not be seen. It is possible that the grooves have been filled out by the deposited platinum or that the image quality is too low for the grooves to be seen. Figures (b) and (c) show the sample looking uneven around the fin. Somehow the two sides of the fins have been affected in different ways by the fabrication process. Figure 18 (d) shows a tilted side view of the same sample as figure 24 (b), before the wet etch. In this figure, the sample looks the same on both sides of the fins. This implies that this unevenness is a result of the wet etch. It will need to be investigated further. A difference between figures 24 (b) and (c) is the sidewalls. In figure (b) the sidewalls have a small slope and skirt out a lot compared to the other cross-sectional images. Figure (c) shows a fin with very smooth sidewalls compared to the other cross-sectional images. This implies that the higher RF power and longer wet etch time that has been used to fabricate this sample generate fins with very smooth sidewalls.

Figure 25 shows images of samples where the trench size can be measured. The size of the trenches, both their depth and width, change with the RF power in the ICP-RIE. As described in section 4.1.1, increasing the RF power in the ICP-RIE process leads to both increased physical and chemical etching components. That section explores how that increase leads to both a higher etch rate and also smoother and therefore thinner fins. However, this increase acts differently on the trenches. To fully explore this difference, the change in the size of the trenches with increased RF power is examined in more detail. In figure 26 the

etch rate of the trenches, in both x and y directions, changes as the RF power in the ICP-RIE process is increased. Etch rates are calculated by dividing the width and depth of trenches by their respective etching times.

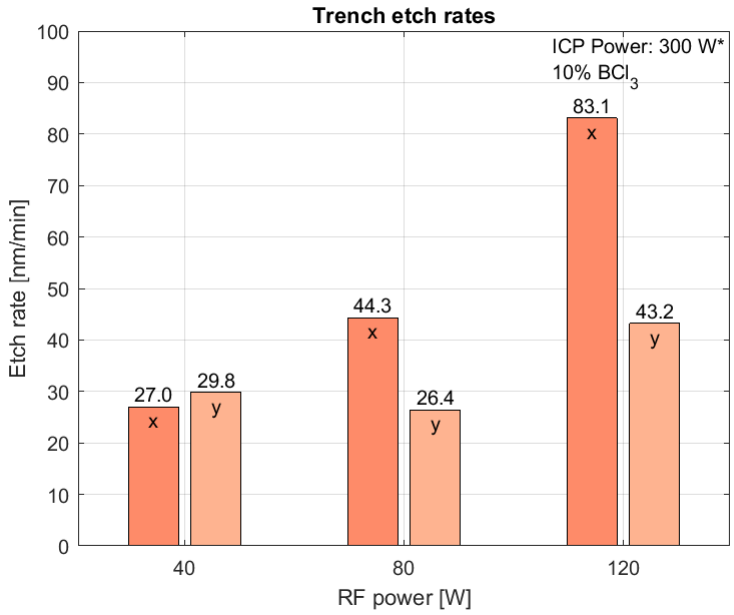

Figure 26: Etching rate variations in the x and y directions of the trenches, resulting from variations in the RF power. The ICP power was kept at 600 W for the 40 W RF power measurement. 300 W for the other RF powers.

Figure 26 shows a strong relationship between the RF power and trench etch rate. However, this relationship does not seem equal for the x and y directions. The etch rate in the x-direction increases greatly as the RF power increases. In the y-direction, this increase is a lot smaller. Contrasting this result, Yue et al. [13] found that the increased RF power led to an equal increase in etch rate for both the x- and y-directions of the trench, which they attribute to the increased physical bombardment. The reason that the etch rate increases more in the x-direction could be that the physical bombardment enhances the chemical etching, as discussed in section 4.1.1. The reason that this result differs from the one presented by Yue Sun, et al [13] could possibly be either difference in RF and ICP powers during etching, a difference in the width and shape of the fins or the fact that different tools always have variations in their condition. Further investigation needs to be done.

4.4 Simulation

Two finite element simulations were carried out in COMSOL to observe the effect of the trenches on the electric field. These simulations were carried out on geometry similar to the fin architecture with the electrical properties of GaN, as voltages are applied at the top and bottom of the structures. 100 V is applied to the bottom of the structure and the top is grounded. A layer of Al_2O_3 is also simulated on top of the fin, as it would be there in a transistor structure. The sides on the base of the simulation are connected, to simulate a series of identical fins next to each other, these simulations can be seen in figures 27 (a) and (b). Boundary conditions and applied voltages are the same in both simulations.

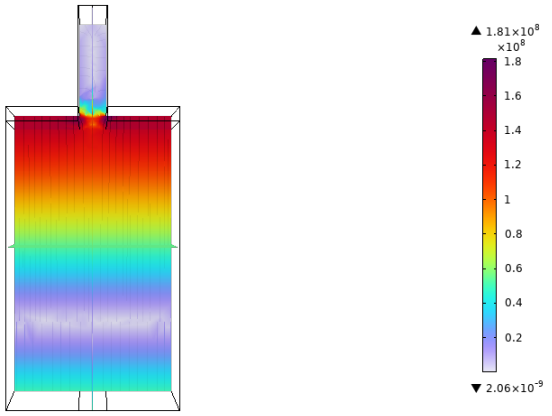

(a) Simulation of fin structure without trenches.

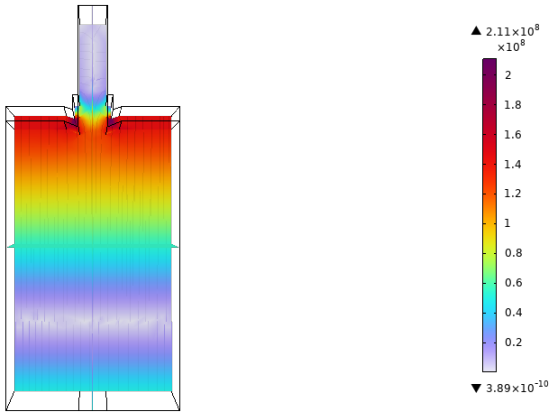

(b) Simulation of fin structure with trenches.

Figure 27: COMSOL finite element simulation of electric field norm, measured in [V/m], in theoretical fin structures. Figure (a) shows a fin without trenches. Figure (b) shows a fin with trenches.

These images show that there is a difference in the electric field over the fin structure with and without trenches. The fin simulated in figure 27 (a) is theoretically perfect, with no trenches, perfectly straight and smooth walls, and sharp corners. The better the etching process becomes, the resulting fins will be closer to this. Figure 27 (b) is a simulation of a fin, closer in shape to the actual resulting fins. These images show how the electric field differs between the fins with and without trenches. In the fin without trenches, the field is concentrated at the surface of the substrate. In the fin with trenches, the field is larger in the trenches, and weaker at the surface of the substrate. The strength of this field is also larger than for the fin without trenches. With the field focused in the trenches, the electric field also reaches higher into the fin, where it reaches further up than for the fin without trenches. This shows that a fin without trenches will be able to create a better transistor. Since the FinFETs work by controlling the flow of electrons through this fin.

5 Conclusions

In the framework of this thesis, the conclusion that is worked towards is a recipe for the ICP-RIE and wet etching steps of the GaN fins. This recipe should be optimized for creating fins with a defined shape, smooth walls, and smaller-sized trenches. For the ICP-RIE etching steps, three parameters were varied. The RF and ICP power as well as the BCl_3/Cl_2 gas ratio.

Increasing the RF power in the ICP-RIE process has had a large impact on the etching of the fins. Resulting in an increased etch rate and also fins with smoother sidewalls. However, increasing the RF power also increases the trench etch rate. The simulation discussed in section 4.4 shows that the trench has a negative influence on the future transistor. The exact influence of the increase in the size of the trench cannot be shown in this thesis, it will need to be investigated further.

Increasing the ICP power of the ICP-RIE process results in an increased etching rate. However, the shape of the fins remains unchanged. The sloped walls and outskirting is not removed. In a similar fashion to this, increasing the ratio of BCl_3 gas results in a decreased etching rate.

To determine whether a variation in the parameters: RF power, ICP power, or BCl_3/Cl_2 gas ratio is a variation that should be made to the etching recipe, their influence on the resulting fins is examined. If a variation is to be worthwhile it should change the resulting fins in a way that would allow for better transistors to be created. This change should not be able to be achieved by varying the etching time. The RF power increase results in fins with smooth and straight sidewalls. Making it a worthwhile change to etching recipe. The ICP power increase leads to the largest increase in etch rate, but it is not a worthwhile change to the etching recipe. Increasing the BCl_3 gas ratio only reduced the etch rate, meaning that it is not a worthwhile change to the recipe.

The wet etch step of the process should for the best results be carried out in a single interval, with the TMAH heated to 40°C. This will result in a complete wet etch.

Finally, an optimized recipe for the etching of GaN for FinFET applications can be proposed. The ICP-RIE process should have an RF power of 120 W, an ICP power of 300 W, and a BCl_3/Cl_2 ratio of 10% BCl_3, with an etching time to achieve the desired fin height with the given etch rate for these conditions. This should be followed by a wet etching step in TMAH, heated to 40°C, for 50 minutes.

References

[1] Zhang Y, Palacios T. (Ultra)Wide-Bandgap Vertical Power FinFETs. IEEE Transactions on Electron Devices. 2020 Oct;67(10):3960-71. Available from: https://ieeexplore.ieee.org/document/9124652/.

[2] Bhattacharya D, Jha NK. FinFETs: From Devices to Architectures. Advances in Electronics. 2014 Sep;2014:1-21. Available from: https://www.hindawi.com/journals/aelc/2014/365689/.

[3] Zhang Y, Dadgar A, Palacios T. Gallium nitride vertical power devices on foreign substrates: a review and outlook. Journal of Physics D: Applied Physics. 2018 Jul;51(27):273001. Available from: https://iopscience.iop.org/article/10.1088/1361-6463/aac8aa.

[4] Meneghini M, De Santi C, Abid I, Buffolo M, Cioni M, Khadar RA, et al. GaN-based power devices: Physics, reliability, and perspectives. Journal of Applied Physics. 2021 Nov;130(18):181101. Available from: https://aip.scitation.org/doi/10.1063/5.0061354.

[5] Zhang Y, Sun M, Perozek J, Liu Z, Zubair A, Piedra D, et al. Large Area 1.2 kV GaN Vertical Power FinFETs with a Record Switching Figure-of-Merit. IEEE Electron Device Letters. 2018:1-1. Available from: https://ieeexplore.ieee.org/document/8528328/.

[6] Auffan M, Santaella C, Thiéry A, Paillès C, Rose J, Achouak W, et al. Electron Beam Lithography (EBL). In: Bhushan B, editor. Encyclopedia of Nanotechnology. Dordrecht: Springer Netherlands; 2012. p. 718-40. Available from: http://link.springer.com/10.1007/978-90-481-9751-4_344.

[7] Williams ER, Faller JE, Hill HA. New Experimental Test of Coulomb's Law: A Laboratory Upper Limit on the Photon Rest Mass. Physical Review Letters. 1971 Mar;26(12):721-4. Available from: https://link.aps.org/doi/10.1103/PhysRevLett.26.721.

[8] Chaichian M, Merches I, Radu D, Tureanu A. The Electromagnetic Field. In: Electrodynamics. Berlin, Heidelberg: Springer Berlin Heidelberg; 2016. p. 115-68. Available from: http://link.springer.com/10.1007/978-3-642-17381-3_3.

[9] Liu Z, Wang Y, Xia X, Yang H, Li J, Gu C. Fabrication of GaN hexagonal cones by inductively coupled plasma reactive ion etching. Journal of Vacuum Science & Technology B, Nanotechnology and Microelectronics: Materials, Processing, Measurement, and Phenomena. 2016 Jul;34(4):041226. Available from: http://avs.scitation.org/doi/10.1116/1.4954986.

[10] Laermer F, Franssila S, Sainiemi L, Kolari K. Deep reactive ion etching. In: Handbook of Silicon Based MEMS Materials and Technologies. Elsevier; 2020. p. 417-46. Available from: https://linkinghub.elsevier.com/retrieve/pii/B9780128177860000165.

[11] Godin B, Touitou E, Krishnan R, Heller MJ, Green NG, Nili H, et al. Dry Etching. In: Bhushan B, editor. Encyclopedia of Nanotechnology. Dordrecht: Springer Netherlands; 2012. p. 587-9. Available from: http://link.springer.com/10.1007/978-90-481-9751-4_353.

[12] Shul RJ, McClellan GB, Casalnuovo SA, Rieger DJ, Pearton SJ, Constantine C, et al. Inductively coupled plasma etching of GaN. Applied Physics Letters. 1996 Aug;69(8):1119-21. Available from: http://aip.scitation.org/doi/10.1063/1.117077.

[13] Sun Y, Kang X, Zheng Y, Wei K, Li P, Wang W, et al. Optimization of Mesa Etch for a Quasi-Vertical GaN Schottky Barrier Diode (SBD) by Inductively Coupled Plasma (ICP) and Device Characteristics. Nanomaterials. 2020 Apr;10(4):657. Available from: https://www.mdpi.com/2079-4991/10/4/657.

[14] Itoh M, Kinoshita T, Koike C, Takeuchi M, Kawasaki K, Aoyagi Y. Straight and Smooth Etching of GaN (1\bar100) Plane by Combination of Reactive Ion Etching and KOH Wet Etching Techniques. Japanese Journal of Applied Physics. 2006 May;45(5A):3988-91. Available from: https://iopscience.iop.org/article/10.1143/JJAP.45.3988.

[15] Sze SM, Lee MK. Semiconductor Devices: Physics and Technology, 3rd Edition. John Wiley & Sons, Inc; 2012.

[16] Tautz M, DíazDíaz D. Wet-Chemical Etching of GaN: Underlying Mechanism of a Key Step in Blue and White LED Production. ChemistrySelect. 2018 Feb;3(5):1480-94. Available from: https://onlinelibrary.wiley.com/doi/10.1002/slct.201702267.

[17] Al Taradeh N, Frayssinet E, Rodriguez C, Morancho F, Sonneville C, Phung LV, et al. Characterization of m-GaN and a-GaN Crystallographic Planes after Being Chemically Etched in TMAH Solution. Energies. 2021 Jul;14(14):4241. Available from: https://www.mdpi.com/1996-1073/14/14/4241.

[18] Zhu Y, Inada H, Hartschuh A, Shi L, Della Pia A, Costantini G, et al. Scanning Electron Microscopy. In: Bhushan B, editor. Encyclopedia of Nanotechnology. Dordrecht: Springer Netherlands; 2012. p. 2273-80. Available from: http://link.springer.com/10.1007/978-90-481-9751-4_110.

[19] Rawal DS, Arora H, Sehgal BK, Muralidharan R. Comparative study of GaN mesa etch characteristics in Cl $_2$ based inductively coupled plasma with Ar and BCl $_3$ as additive gases. Journal of Vacuum Science & Technology A: Vacuum, Surfaces, and Films. 2014 May;32(3):031301. Available from: http://avs.scitation.org/doi/10.1116/1.4868616.

A Sample Fabrication Process Worksheet

In this section, a worksheet detailing the entire sample fabrication process can be seen. This worksheet has been continuously followed and updated during this thesis as the individual samples have been fabricated.

(a) Page one (b) Page two (c) Page three

Figure 28: Worksheet showing the complete experimental process steps and how individual samples have been fabricated. Each row corresponds to a process step and each column corresponds to information about said step, or about a specific sample.

Figure (a) shows all steps in the experimental process, together with an explanation of the activity, tool used as well as additional comments. Figures (b) and (c) show what steps have been completed on what samples. A green box indicates that the step has been completed without complications. A grey box indicates that the step has been completed with some complication. Additional comments can be seen in these grey boxes. The row with orange borders shows values of the variable parameters for the ICP-RIE etching step, RF power, ICP power, BCl_3/CL_2 gas ratio and etching time. These boxes has been filled out continuously during the thesis, as the steps have been completed.